1

Counter Electrode Catalysts in Dye-Sensitized Solar Cells – An Overview

Sining Yun

Xi'an University of Architecture and Technology, Functional Materials Laboratory (FML), School of Materials & Mineral Resources, No. 13 Yanta Road, Xi'an, Shaanxi Province, 710055, China

In this chapter, we will give an overview on the counter electrode (CE) catalysts in dye-sensitized solar cells (DSSCs). The contents in this chapter include (i) history and cell efficiency level of DSSCs, (ii) fabrication techniques of a DSSC and a symmetrical dummy cell, (iii) the operating principle of a DSSC, (iv) the operating principle of a CE catalyst in DSSCs, (v) types and advances in CE catalysts in DSSCs, and (vi) general design consideration of this book.

1.1 History and Cell Efficiency Level of DSSCs

Over the past 20 years, DSSCs as new-generation solar cells have drawn much attention because of their low cost, simple fabrication, and high solar-to-electrical power conversion efficiency (PCE) as compared with silicon-based and thin film solar cells. The earliest DSSCs can be dated back to the pioneering work of Gerischer and Tributsch in the late 1960s, and they found that the organic dyes adsorbed on ZnO single-crystal electrodes can produce photocurrents [1–3]. Subsequently, Tributsch and Calvin further demonstrated that the sensitized ZnO semiconductors play a key role in solar energy conversion [3–5]. The PCEs of this type of electrochemical cell are much lower at that time, which has not drawn wide public attention in many labs around the world [1, 6–8]. Approximately 10 years later, in 1977, the use of rutile TiO_2 electrode in this electrochemical cell resulted, in the turn of the tide, in the improvement of cell performance [6, 9]. Many researchers from various groups worldwide devote themselves to the study of electrochemical cells. A big breakthrough was then made, and a high PCE of 7.1–7.9% was reported in the famous 1991 Nature paper by O'Regan and Grätzel [10]. Thereafter, type of electrochemical cell was named DSSCs (or Grätzel cell) because of the use of mesoporous TiO_2 semiconductor with a large specific surface area. This new and revolutionary thin film solar cell initiated a new era of research and development of low-cost and high-performance DSSCs.

Counter Electrodes for Dye-Sensitized and Perovskite Solar Cells,
First Edition. Edited by Sining Yun and Anders Hagfeldt.

A typical DSSC is composed of a dye-sensitized mesoscopic TiO_2 photoelectrode (PE), a iodide/triiodide (I^-/I_3^-) redox couple electrolyte, and a platinized CE catalyst. Each component of the DSSCs performs a specific task and the whole performance of DSSCs strongly depends on the optimization of the individual cell components in a DSSC system. Over the past two decades, great progress has been made in fundamental research and technological application of DSSCs [11–33]. In a new DSSC system, alternative CE catalysts, sensitizers (N719, Z907, N3, D35, Y123, etc.), and redox couples (I_3^-/I^-, Co^{2+}/Co^{3+}, T_2/T^-, and Cu^{2+}/Cu^+) were employed for practical and economic considerations. To meet the compatibility or match the demands of different cell components of DSSCs, all cell components of DSSCs must have to be carefully selected to achieve the superior DSSC performance. Tremendous advances in the cell efficiency level of DSSCs have been made, as summarized in Table 1.1. The PCE value of DSSCs increased from 7.12% in 1991 to 13% in 2014, and a champion PCE value of 14.3% was obtained in 2015 for cobalt-mediated DSSCs with graphene nanoplatelet (GNP) CEs and combined photosensitizers of ADEKA-1 and LEG4 dyes. More comments on the match issues of the cell components of DSSCs have been analyzed and reviewed in the previous literature [11, 54–57].

Although the cell efficiency level has been nearly similar to the standard values (15%) for practical applications, the present efficiency level is not evidently satisfactory for large-scale application in a broader photovoltaic market, especially considering the stability such as the electrochemical stability, the mechanical stability, and the long-term stability [55–57]. Therefore, it is highly desired for achieving more efficient and more stable DSSC components. Additionally,

Table 1.1 The PCE values in DSSCs with various cell components (100 mW cm^{-2}, AM 1.5 G).

No.	PE‖CE‖Redox couple‖Dye	Dye type	Area (cm^2)	PCE (%)	References
1	TiO_2/Pt/(I_3^-/I^-)/trimeric Ru dye	Ru dye	0.50	7.9	[10]
2	TiO_2/Pt/(I_3^-/I^-)/N3	Ru dye	0.31	10.0	[34]
3	TiO_2/Pt/(I_3^-/I^-)/N719	Ru dye	0.1697	10.0	[35]
4	TiO_2/Pt/(I_3^-/I^-)/N719	Ru dye	0.158	11.18	[36]
5	TiO_2/Pt/(I_3^-/I^-)/(black dye)	Ru dye	0.219	11.1	[37]
6	TiO_2/Pt/(I_3^-/I^-)/CYC-B11	Ru dye	0.158	11.5	[38]
7	TiO_2/Pt/(I_3^-/I^-)/C106	Ru dye	0.158	11.7	[39]
8	TiO_2/Pt/(I_3^-/I^-)/(black dye + Y1)	Ru dye	0.231	11.4	[40]
1	TiO_2/Pt/(I_3^-/I^-)/indoline dye 1	Organic dye	0.16	8.00	[41]
2	TiO_2/Pt/(I_3^-/I^-)/D149	Organic dye	—	9.03	[42]
3	TiO_2/Pt/(I_3^-/I^-)/D205	Organic dye	—	9.52	[43]
4	TiO_2/Pt/(I_3^-/I^-)/C219	Organic dye	0.158	10.1	[44]
5	TiO_2/Pt/(I_3^-/I^-)/JF419	Organic dye	0.20	10.3	[45]
1	TiO_2/Pt/(I_3^-/I^-)/Cu-2-α-oxymesoisochlorin *e*4	Porphyrin dye	0.50	2.6	[46]

(Continued)

Table 1.1 (Continued)

No.	PE‖CE‖Redox couple‖Dye	Dye type	Area (cm^2)	PCE (%)	References
2	TiO_2/Pt/(I_3^-/I^-)/TCPP	Porphyrin dye	1.00	3.5[a)]	[47]
3	TiO_2/Pt/(I_3^-/I^-)/Zn-3	Porphyrin dye	—	5.6	[48]
4	TiO_2/Pt/(I_3^-/I^-)/ZnTPMA-2	Porphyrin dye	—	7.1[b)]	[49]
5	TiO_2/Pt/(I_3^-/I^-)/YD-2	Porphyrin dye	0.16	11	[50]
6	TiO_2/Pt/(Co^{3+}/Co^{2+})/ (YD2-*o*-C8+Y123)	Porphyrin dye	0.36	12.3	[51]
7	TiO_2/GNP/(Co^{3+}/Co^{2+})/SM315	Porphyrin dye	0.28	13	[52]
8	TiO_2/GNP/(Co^{3+}/Co^{2+})/ (ADEKA-1 +LEG4)	Organic dye	0.1024	14.3[c)]	[53]

a) TCPP: *tetra*(4-carboxyphenyl)porphyrin.
b) ZnTMPA: zinc tetraarylporphyrin malonic acids.
c) ZnTMPA: the photocurrent–voltage (J–V) properties of the cells with maintaining the aperture area of the cells to be $0.32 \times 0.32\ cm^2$ by the use of a square black shade mask with a thickness of 30 μm.

almost all CE materials (carbon materials, polymers, transition metal compounds (TMCs), and their corresponding hybrids) have their own merits and demerits; therefore, it is often difficult to decide which one is better than the other even if the dye and the electrolyte were not decided in the DSSC systems. This indicated that the optimized and well-matched cell components within the DSSC devices are also highly desired for making a significant breakthrough in cell efficiency level. A maximum PCE of slightly higher than 30% can be achievable by harvesting ultraviolet (UV) to near infrared ray (IR) photons, to transform the DSSC into a mature commercial technology, similar to silicon-based and thin film solar cell technologies [27, 57].

1.2 Fabrication Techniques of a DSSC and a Symmetrical Dummy Cell

1.2.1 Preparation of Photoelectrode

Mesoscopic TiO_2 photoelectrodes (PEs), CE catalysts, and electrolytes were prepared separately and then assembled in a DSSC device. A 12-μm-thick TiO_2 (P25; Degussa, Germany) film with a grain size of 20 nm was coated on an fluorine-doped tin oxide (FTO) glass substrate using screen printing technique. The obtained film was annealed at 500 °C for 30 minutes and then cooled to 80 °C. The resulting TiO_2 films were immersed in 0.5 mM solution of N719 dye (Solaronix SA, Switzerland) in ethanol solution for 20 hours to obtain the dye-sensitized mesoscopic TiO_2 photoanode. The fabrication process of PEs is similar to that reported in our previous literature [55, 56, 58–64]. In some cases, $TiCl_4$ solution pre- and post-treatment was used to allow the formation of a thin and compact TiO_2 underlayer and increase the surface area of the TiO_2 particles [65].

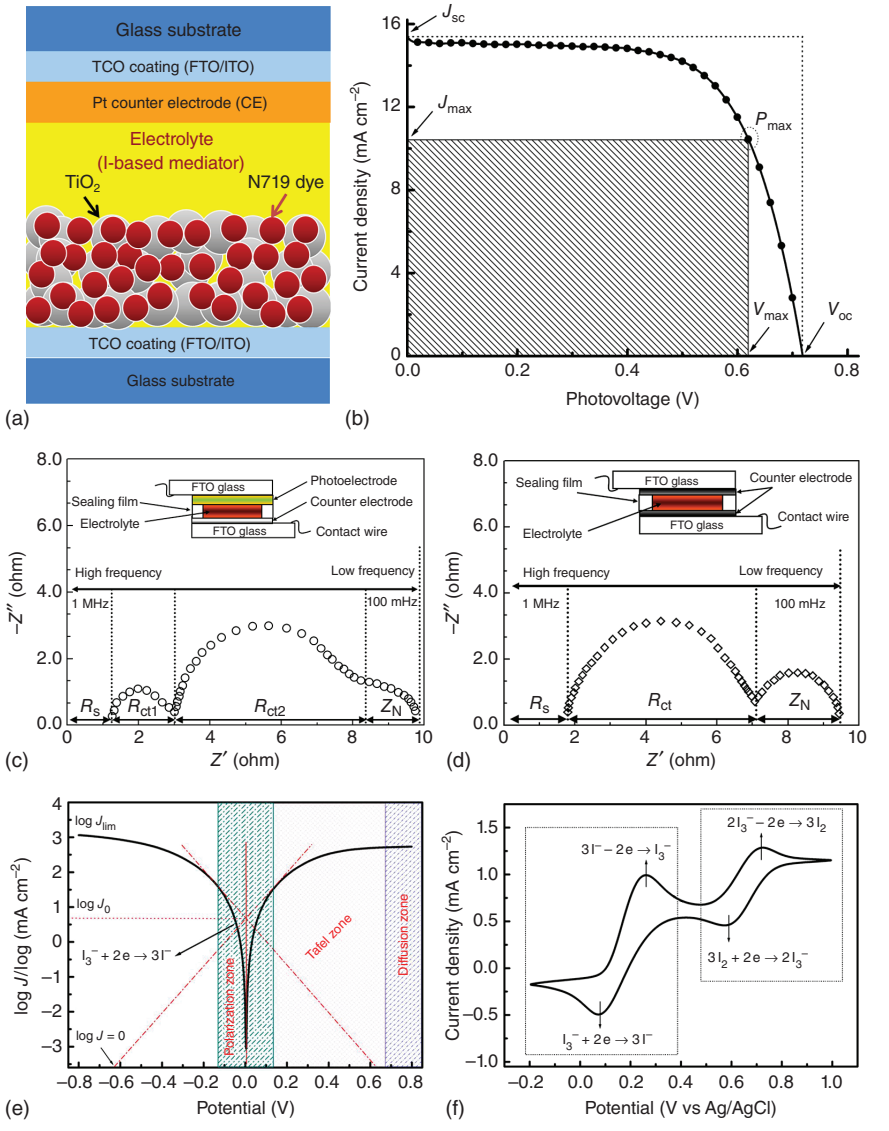

Figure 1.1 (a) A schematic illustration of the fabrication of a sandwich-type DSSC. (b) Photocurrent density–photovoltage (*J*–*V*) curves for DSSCs. (c) Nyquist plots for the DSSCs fabricated with PE and CE catalysts. The inset is a schematic illustration of a sandwich-type DSSC. (d) Nyquist plots for the symmetrical cells fabricated with two identical CE catalysts. The inset is a schematic illustration of the symmetrical cells. (e) Tafel curves for the symmetrical cells fabricated with two identical CE catalysts. (f) Cyclic voltammetry (CV) of iodide/triiodide (I^-/I_3^-) redox couple electrolyte for Pt electrodes with an electrolyte solution composed of $LiClO_4$ (0.1 M), LiI (10 mM), and I_2 (1 mM) in acetonitrile. A Pt electrode was used as the CE and Ag/Ag^+ as the reference electrode.

1.2.2 Preparation of Counter Electrodes

Pt CE of DSSCs was prepared by pyrolyzing platinum acid chloride isopropyl alcohol solution ($H_2PtCl_6 \cdot 6H_2O$ dissolved in isopropyl alcohol solution) at 500 °C for 30 min under air atmosphere. For more strategies of Pt CE fabrication, please refer the previous literature [66–69]. For Pt-free CEs, 300 mg of prepared CE powder and 6 g of ZrO_2 pearl were dispersed in 6 ml isopropanol and milled for four hours. The obtained CE solution was then sprayed on an FTO glass substrate (type-U, 14 Ω sq^{-1}; Asahi Glass, Japan) using an airbrush (TD-128; Tiandi Co., Ltd.). The FTO glass substrate, coated with Pt-free CE film, was then annealed under a N_2 atmosphere at 400 °C for 30 minutes in a tube furnace. The expected CEs were obtained. For more strategies of Pt-free CE fabrication, please refer the previous literature [55, 56, 70–72].

1.2.3 Cell Fabrication

The PEs and CEs were assembled in a dry box with 25 or 35 μm of Surlyn (Dupont), which provides spacing between the two electrodes and sealing for the electrolyte. The electrolyte, containing 0.06 M LiI, 0.03 M I_2, 0.6 M 1-butyl-3-methylimidazolium iodide, 0.5 M 4-*tert*-butyl pyridine, and 0.1 M guanidinium thiocyanate in acetonitrile solution, was introduced into the device through a predrilled hole in the CE under vacuum. The active area of a sandwich DSSC is usually 0.16 cm^2. A schematic illustration of the fabrication of a sandwich-type DSSC is illustrated in Figure 1.1a [10, 18]. The as-assembled DSSCs were used for testing the photovoltaic performance of cells (Figure 1.1b). The as-assembled DSSCs were used in electrochemical impedance spectroscopy (EIS) (Figure 1.1c).

The symmetrical dummy cell was fabricated by two identical CEs. Then, the electrolyte, containing 0.06 M LiI, 0.03 M I_2, 0.6 M 1-butyl-3-methylimidazolium iodide, 0.5 M 4-*tert*-butyl pyridine, and 0.1 M guanidinium thiocyanate in acetonitrile solution, was filled in the symmetrical dummy cell and sealed with the established process, as mentioned above. The as-fabricated symmetrical cells were used in EIS and Tafel polarization tests, as shown in Figure 1.1d and e. Cyclic voltammetry (Figure 1.1f) was performed on an electrochemical analyzer in a three-electrode system in an argon-purged acetonitrile solution containing 0.1 M $LiClO_4$, 10 mM LiI, and 1 mM I_2. Pt electrode is used as a CE and Ag/Ag^+ works as a reference electrode. The electrochemical properties of CEs at frequencies ranging from 100 mHz to 1 MHz were measured with a computer-controlled potentiostat at the bias potential (−0.75 V) and the AC amplitude (10 mV).

1.3 Operating Principle of DSSCs

A schematic illustration of operating principles of a sandwich-type DSSC system is shown in Figure 1.2. In this sandwich-type DSSC, the dye molecule absorbs light and generates charge carriers. Under solar illumination, the incoming

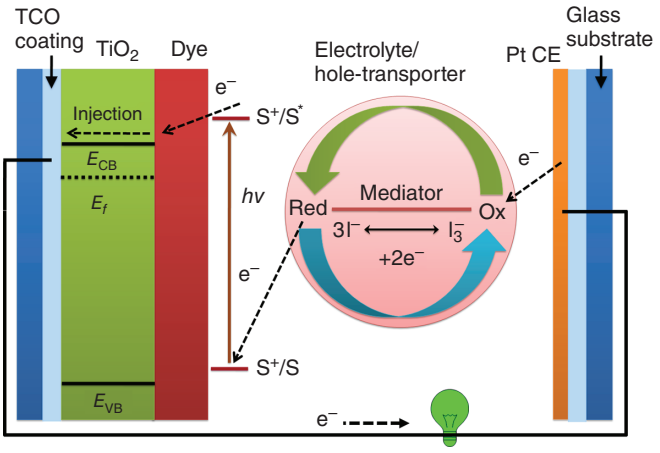

Figure 1.2 A schematic illustration of the working principle of a sandwich-type DSSC. Source: Yun et al. 2016 [73]. Reproduced with permission of Elsevier.

photons are captured by the dye molecules. Sensitizer molecules adsorbed onto the surface of TiO_2 film are excited from the ground state (S) to the excited state (S*) and rapidly injected an electron into the conduction band of the semiconducting TiO_2, thus leaving a hole in the sensitizer (S^+). The injected electrons are transported through an external circuit to reach the CE. The regeneration of the dye molecules and the electrolyte is finished during the photoelectric transformation process. S^+ was reduced to S by I^- ions, whereas the electrolyte itself is regenerated by I_3^- reduction at the CE surface. The electrons diffuse through the network-structured TiO_2 film to reach the external load on the surface of the CE. In a solid-state DSSC, the dye molecule is regenerated by the hole transporter instead of the liquid redox couple. Totally, the basic working principle of solid-state DSSCs is similar to that of liquid-state DSSCs. More details on the operating principles of a DSSC can be found in the previous literature [13–18, 20].

1.4 Operating Principle of a Counter Electrode in DSSCs

As a crucial component of DSSCs, the CE plays a critical role in the operation of DSSCs. As illustrated in Figure 1.3, the CE has two roles. Firstly, the CE must efficiently promote the electron transfer from the external circuit back to the electrolyte. Secondly, the CE can catalyze the I_3^- reduction into the I^- ions at the CE/electrolyte interface. Therefore, superior catalytic activity and high electrical conductivity are highly desired for CE catalysts. However, it is difficult for one CE material to exhibit both high electrical conductivity and catalytic activity required for efficient work.

In a traditional DSSC, the CE is traditionally composed of Pt materials. However, Pt metal is of high cost and scarce, and the limited supply of Pt cannot meet the increasing demand for its practical applications. In addition, Pt is

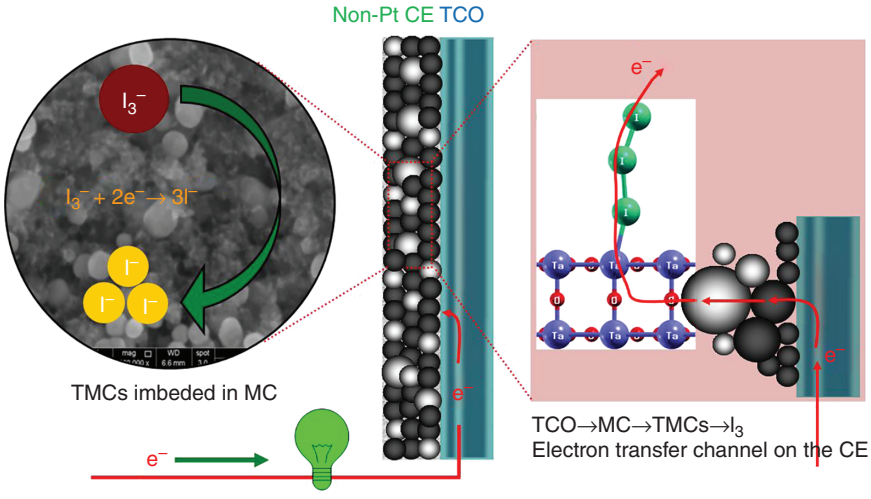

Figure 1.3 A schematic illustration of the operation principle of a CE in a DSSC. In this DSSC with N719 dye and the iodide/triiodide (I^-/I_3^-) redox couple electrolyte, transition metal compounds (TMCs, such as TaO and TaC) imbedded the mesoporous carbon (MC), TaO/MC, and TaC/MC were used as the CE catalysts. Source: Yun et al. 2014 [55]. Reproduced with permission of John Wiley & Sons.

not very effective as a CE catalyst for redox couples such as cobalt complexes, T_2/T^-, and polysulfide electrolytes. To overcome this challenge, developing high-performance, Pt-free CE catalytic materials is an effective strategy to provide high electrical conductivity and superior catalytic activity simultaneously [11, 54–57, 67–69, 73–78].

1.5 Types and Advances in Counter Electrodes in DSSCs

1.5.1 Types of Counter Electrodes in DSSCs

As far as the CE catalysts are concerned, (i) better catalytic activity, (ii) better electrical conductivity, (iii) better chemical stability, (iv) large specific surface area, (v) high corrosion resistance, (vi) better matching, and so on were required for high-performance DSSCs, which must be particularly considered in the design of Pt-free catalysts to maximize the function of CEs. New CE catalytic materials are rapidly developing as an alternative Pt electrode in DSSCs. Six types of CE materials, such as Pt metal, metal and alloy, conducting polymers, carbon materials, TMCs, and hybrids, have been developed so far for DSSC systems (Figure 1.4a). To make full use of the synergistic catalytic effect resulting from various components of the hybrid materials, seven types of hybrid CE catalysts (Figure 1.4b), such as carbon/carbon, TMCs/TMCs, polymers/polymers, carbon/TMCs, carbon/polymer, polymer/TMCs, and TMCs/polymer/carbon, have been developed and employed in DSSCs [55–57]. Pt metal electrode has established itself as the preferred CE catalytic material in DSSC due to its high catalytic activity. In order to utilize the peculiarity of Pt metal and reduce the cost of CE catalysts in DSSCs,

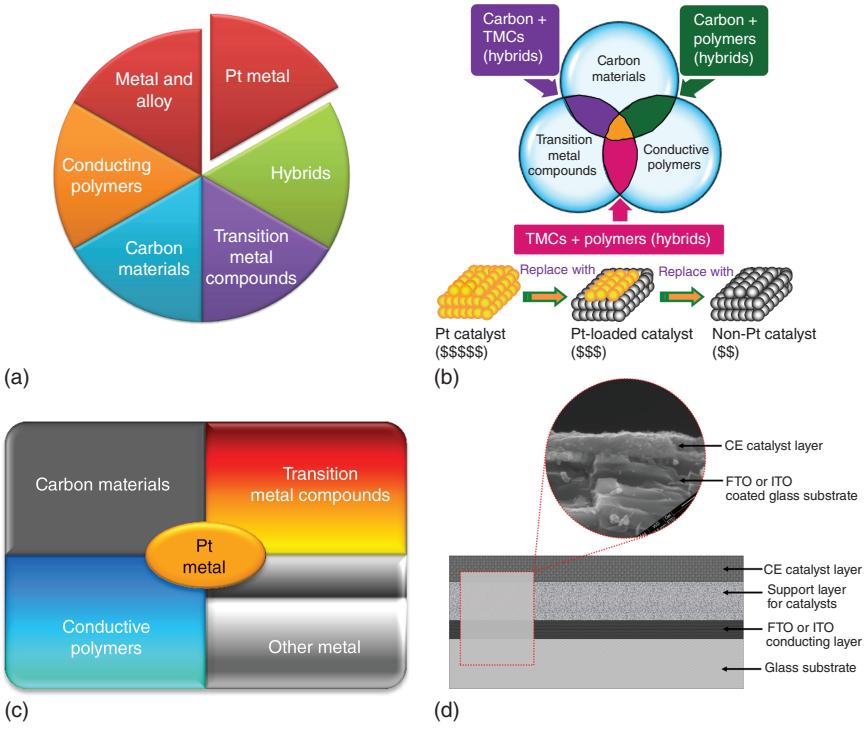

Figure 1.4 (a) Six types of CE catalysts employed in DSSCs; (b) seven types of hybrid CE catalysts (carbon/carbon, TMCs/TMCs, polymers/polymers, carbon/TMCs, carbon/polymer, polymer/TMCs, and TMCs/polymer/carbon) employed in DSSCs; (c) four types of Pt-loaded CE catalysts (Pt/carbon, Pt/polymer, Pt/TMC, and Pt/metal) employed in DSSCs; and (d) the structural sketch of hybrid CE catalysts in DSSCs.

one possible approach is to reduce the required amount of Pt metal on CE surface by developing Pt-loaded hybrid catalysts, as illustrated in Figure 1.4c. This strategy further opens up the possibility of cost reduction of the DSSC devices, which is vital to promote large-scale applications of DSSCs [60, 79, 80]. Among these CE catalytic materials, the hybrid CEs are composed of a glass substrate, a conducting layer, a support layer, and a CE catalyst layer (Figure 1.4d) that have drawn much attention because of their peculiar structure and their synergetic catalytic effects resulting from various components of the hybrid CE materials.

1.5.2 Advances in Counter Electrode in DSSCs

Until now, great progresses have been made in the CE catalysts in DSSCs. Typical PCE values of I-mediated DSSCs using various CE catalysts (presented in Figure 1.4) are demonstrated in Figure 1.5a and b, and the corresponding photovoltaic parameters of DSSCs were summarized in the Appendix: *Cell Efficiency Table of DSSCs with Various Counter Electrode Electrocatalysts*. For noble Pt electrodes listed in Table 1.1, although it is preferred that CE catalytic

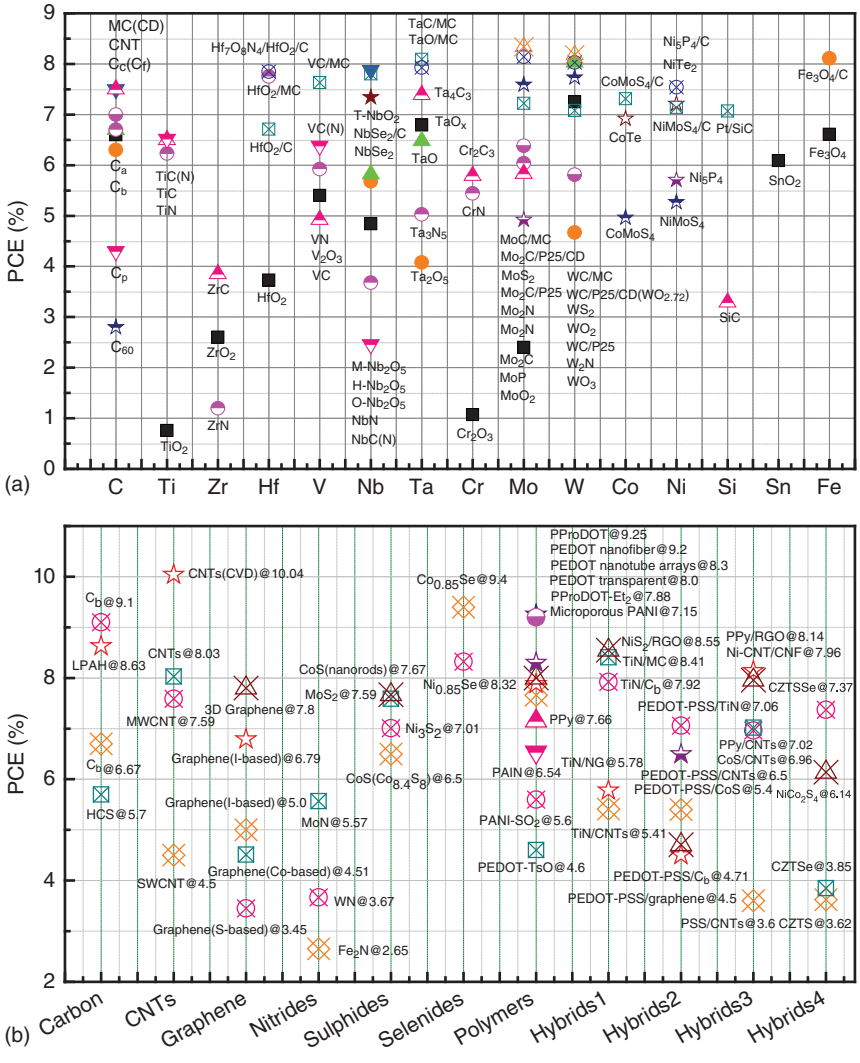

Figure 1.5 PCE values of I-mediated DSSCs used carbon materials and transition metal compounds as typical CE catalysts resulted from two groups (Prof. Tingli Ma and Prof. Sining Yun) (a); and by other groups (b) [55]. The corresponding photovoltaic parameters of DSSCs were summarized in the Appendix: *Cell Efficiency Table of DSSCs with Various Counter Electrode Electrocatalysts*. Source: Yun et al. 2014 [55]. Reproduced with permission of John Wiley & Sons.

materials in I-mediated DSSCs and higher PCE values can be achieved in most cases, the highest PCE values of DSSCs (14.3%) are based on the new system using the GNP catalyst and the iodine-free electrolyte. This means that the superior performance of DSSCs strongly depends on the optimized and matched cell components (Table 1.1), and the matching should be carefully considered in the design of the CE catalytic materials. For more details on Pt electrode, please refer Chapters 2 and 9.

1.5.2.1 Advances in Carbon Materials in DSSCs

Conventional carbon materials are preferred CE catalytic materials that can achieve higher PCE value in I-mediated DSSCs. However, a large amount of carbon is desired highly to fully reach the performance level of Pt electrodes, which resulted in a bulky and opaque DSSC device. Conventional carbon CE catalysts also suffer from poor adhesion between the CE catalytic layer and the FTO substrate. The demerits of these carbon CEs will further limit their practical applications. A special consideration has been given to the improvements in transparency and adhesion of CE catalytic films in Chapters 4–6. By contrast, carbon nanotubes (CNTs) and graphene are suitable catalytic materials for I_3^- reduction due to their distinctive structures and properties and can be applied for Pt-free CE catalysts in DSSCs [70, 81]. The number of oxygen functional groups and the C:O ratio play a key role in improving catalytic activity in DSSCs for graphene CEs, whereas the preparation methods of CE catalysts and the fabrication process of CNTs are crucial to high-performance DSSCs. A PCE of 10.04% has been achieved in DSSCs using CNTs as CEs that were grown directly on a FTO substrate using a chemical vapor deposition (CVD) technique [82].

1.5.2.2 Advances in Transition Metal Compounds in DSSCs

We have clearly found that almost all transition metal (Ti, Zr, Hf, V, Nb, Ta, Cr, Mo, W, Co, Ni, Si, Sn, Fe, etc.) compounds have been investigated and tested as catalysts in DSSCs (Figure 1.5a). This design idea is based on the fact that these TMCs have similar electronic structures of Pt metal and is able to present Pt-like catalytic activity [83, 84]. Most transition metal oxides present the superior catalytic properties and can be used as CE catalysts in DSSCs. However, not all oxides, such as TiO_2, SnO_2, Nb_2O_5, and WO_3, are promising CE catalytic materials because the energy levels or bandgaps of these oxides may be more preferable for use as a photoanode, not as a CE catalyst or a cathode, in DSSCs. For transition metal oxides, on the one hand, massive oxygen vacancies introduced by nonstoichiometric effect should play a crucial role for enhanced catalytic activity of CE catalysts in DSSCs [85, 86]. On the other hand, the low ratio of oxygen to metal atom of transition metal oxides favors the catalytic activity of these CE catalysts in DSSCs [59, 85, 87, 88].

For transition metal carbides and nitrides, they presented more superior catalytic activity in S-mediated DSSCs than in I-mediated DSSCs (see Appendix). Ta_4C_3 CE showed a higher PCE of 7.39% in DSSCs, reaching 97.6% of the level obtained using a Pt CE (7.57%). Ta_4C_3 is the best carbide CE material in DSSCs as compared to other transition metal carbides [61, 89]. The PCE of DSSCs with Ta_3N_5 (5.03%) CE is much higher than that of DSSCs with WN (3.67%), Fe_2N (2.65%), ZrN (1.20%), and NbN (3.68%) [61, 89, 90]. Highly ordered TiN nanotube arrays on metallic Ti foil substrates as CEs in DSSCs yielded a PCE of 7.73% [91]. Hierarchical TiN spheres coated onto Ti foil as a CE in DSSCs yielded a PCE of 7.83% [92].

Lots of sulfides, such as CoS, $Co_{8.4}S_8$, Co_9S_8, Ni_3S_2, FeS_2, MoS_2, and WS_2, as alternative CE materials have yielded promising photovoltaic performances with PCE values ranging from 6.50% to 7.73% [93–100]. Among them, cobalt sulfide has drawn a massive research attention in the application of CE catalysts

in DSSCs. Note that the morphology of sulfide CE catalytic materials has a considerable effect on the photovoltaic performances of DSSCs. Moreover, CoS is not a preferred CE catalytic material in T-mediated DSSCs as compared with typical I-mediated DSSCs in a single-minded pursuit of high PCE.

For selenide CE catalysts, in-situ-grown $Co_{0.85}Se$ exhibited higher electrocatalytic activity for I_3^- reduction and generated a PCE of 9.40% [101]. $NiSe_2$ prepared using a simple hydrothermal method as a CE yielded a PCE of 8.69% in DSSCs [102]. Use of $NbSe_2$, CoTe, and $NiTe_2$ as CEs in DSSCs achieved PCEs of 7.34%, 6.92%, and 7.21%, respectively, comparable to that of DSSCs with Pt CEs. By contrast, phosphides were only used as one component in hybrid CE catalysts [103, 104].

In general, typical fabrication techniques, for example, urea–metal route (or one-pot method), soft-template route, nano-ink technique, ion exchange technique, and in situ technique, can be used to prepare the TMC catalytic materials. By contrast, the TMCs prepared by one-pot method do not show controllable morphologies as compared with those synthesized through in situ growth and the ion exchange technique. The in situ growth is an effective technique for fabricating morphology-controllable CE materials, which are highly desirable for the tailor-made design based on the relationship between microscopic structure and macroscopic performance. However, the quantity of amorphous carbon (one-side product) in the final product cannot be effectively avoidable and controlled in the preparation of TMCs by the one-pot method.

1.5.2.3 Advances in Polymers in DSSCs

Conjugated polymers have drawn considerable interest as alternative CE catalysts in DSSC systems due to ambient temperatures used in their synthesis as well as conducting nature and facile deposition methods [68, 69, 73, 105, 106]. Polypyrrole (PPy), polyaniline (PANI), poly(3,4-propylenedioxythiophene) (PProDOT), poly(3,4-ethylenedioxythiophene) (PEDOT), and polystyrene-sulfonate-doped poly(3,4-ethylenedioxythiophene) (PEDOT-PSS) have presented good catalytic properties for I_3^- reduction and exhibited a relatively high photovoltaic performance, as presented in Figure 1.6. Microporous PANI CE films exhibited higher catalytic activity for I_3^- reduction and resulted in a PCE of 7.15%, higher than the Pt CE in DSSCs at the same conditions [107]. By contrast, oriented PANI nanowire arrays grown by in situ synthesis exhibit much better catalytic properties in Co-mediated DSSCs with a typical D-π-A organic dye sensitizer (FNE29) than in I-mediated DSSCs with N719 dye, yielding a PCE of 8.24% in DSSCs with the Co^{2+}/Co^{3+} redox couple [108]. Note that PANI is not an ideal CE catalytic material for I-mediated DSSCs because of its instability, self-oxidation, and carcinogenic properties.

For porous PProDOT polymer prepared using electrical-field-assisted growth technique, as-prepared PProDOT CE films yielded PCEs ranging from 9.12% to 9.25% in I-mediated DSSCs. As the Y123 dye was used in Co-mediated DSSCs with PProDOT CEs, the DSSCs produced a V_{oc} close to 1 V and a high PCE of 10.08% [109, 110]. These improvements in photovoltaic performances can be attributed to the ionic liquids used in the electrolyte and the ultralarge surface area of PProDOT films that can eliminate passivation of the interface between

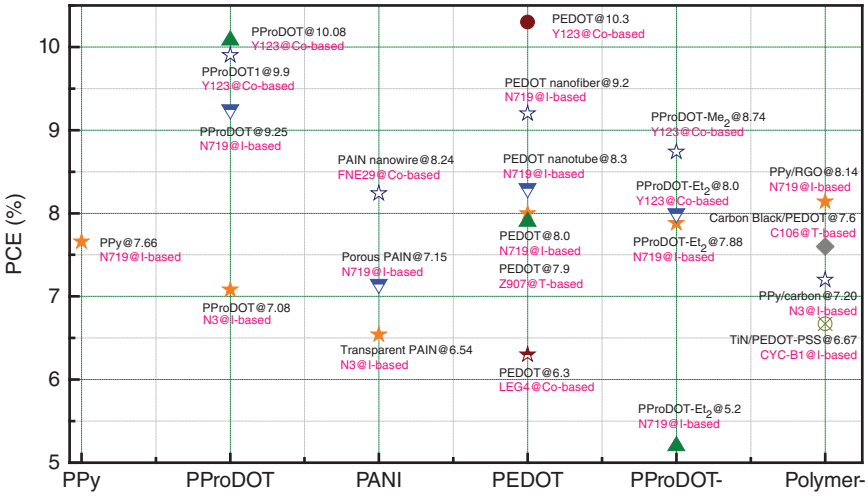

Figure 1.6 Typical PCE values of DSSCs employing polymer-based CEs [73]. The corresponding photovoltaic parameters of DSSCs were summarized in the Appendix: *Cell Efficiency Table of DSSCs with Various Counter Electrode Electrocatalysts*. Source: Yun et al. 2016 [73]. Reproduced with permission of Elsevier.

the CE layer and the electrolyte. In addition, the PEDOT as CE catalysts, a PCE of 8.0% was achieved in acetonitrile-based DSSCs [111]. The PEDOT nanotube arrays, electropolymerized onto ZnO nanowire array templates using the chemical polymerization, as a CE catalyst exhibited a higher catalytic activity for I_3^- reduction than the Pt electrode, resulting in a PCE of 8.3% in DSSCs [112]. By contrast, the PEDOT nanofibers, prepared by a chemical oxidative technique, presented a PCE of 9.2%, higher than bulk PEDOT (6.8%) and Pt electrodes (8.6%) [113]. These results mean that controllable morphology is highly desirable for achieving the high-performance DSSCs for polymer CE catalysts.

One key problem for the PEDOT is that it can form charge transfer complexes with iodide and decrease the performance of DSSCs. To solve this problem, a T_2/T^- redox couple was used as an alternative to the I_3^-/I^- redox couple, a large surface area PEDOT electrode as a CE catalyst yielded a PCE of 7.9% in DSSCs with an optimized T_2/T^- redox electrolyte and a Z907 dye [93, 114]. Another alternative to the I_3^-/I^- redox couple is the Co^{2+}/Co^{3+} redox couple, PEDOT as a CE yielded a PCE of 10.30% in DSSCs with a Y123 dye [115]. These results imply that the T_2/T^- and Co^{2+}/Co^{3+} redox couples have great potential for practical application in DSSCs using PEDOT as a CE catalyst. We want to further stress that PSS, TsO, SO_4^{2-}, ClO_4^-, Cl^-, and BF_4^- as the dopants in the design of polymer CE catalysts have a remarkable effect on the morphologies, electrochemical properties, and photovoltaic performance of devices [73, 106, 116–118]. For more details, please refer our recent review paper [73].

Generally, polymer CE catalysts possess many excellent performance characteristics, such as transparency, flexibility, availability, low cost, high catalytic activity, and high PCE values, which are as good as or even much better than Pt electrode in DSSCs. In addition, most polymer CE catalysts have better match

and adaptability in I-, Co-, and T-based DSSCs with Y123, FNE29, N719, Z907, and N3 dyes. Transparent PEDOT and PProDOT polymers as CE catalysts have been used in flexible and bifacial DSSCs that can absorb incident photons from both sides, resulting in enhanced light absorption [73, 111, 119, 120]. These important contributions will significantly propel future research related with conductive polymers in high-performance and low-cost DSSC systems.

1.5.2.4 Advances in Hybrids in DSSCs

As we mentioned above, the purpose of the hybrid CE design is to make full use of synergetic catalytic effects resulted from different components of the hybrids to further improve the performance of CEs. At the present stage, hybrid CE catalytic materials have become the most popular class of alternative Pt catalytic materials. As demonstrated in Figure 1.4 and 1.5b, carbon materials, polymers, and TMCs are often used as components of the hybrids. Two-component hybrids (TMCs/carbon, carbon/polymers, TMCs/polymers, carbon/carbon, polymers/polymers, and TMCs/TMCs) and three-component hybrids (carbon/TMCs/polymers) are very impressive as Pt-free hybrid CE catalytic materials in DSSCs. In general, the photovoltaic performance of DSSCs can be greatly enhanced using hybrid CE catalysts. For example, DSSCs with hybrid CEs had PCEs close equal to or higher than those using TMCs, RGO, and Pt electrode: (i) I-meditated DSSCs with N719 dye: NiS_2/RGO(8.55%) > Pt(8.15%) > NiS_2(7.02%) > RGO(3.14%); (ii) Co-mediated DSSCs with FNE29 dye: Ta_3N_5/RGO(7.85%) > Pt(7.59%) > RGO(4.55%) > Ta_3N_5(2.89%) and Pt(7.91%) > TaON/RGO(7.65%) > RGO(4.62%) > TaON(2.54%) [121–123]. In addition, WC/MC, MoC/MC, WO_2/MC, TaO/MC, TaC/MC, VC/MC, and HfO_2/MC, as carbon-based hybrid CEs, presented PCEs of 8.18%, 8.34%, 7.76%, 8.09%, 7.93%, 7.63%, and 7.75%, respectively [58, 62, 89, 124, 125]. The PCE values are higher than the corresponding TMCs and MC CE catalysts.

As CE catalyst in DSSCs, TiN/CNTs hybrids resulted in comparable photovoltaic performance with the Pt electrode (5.41% vs 5.68%) [126]. TiN/C_b (C_b: carbon black) hybrid CE catalysts show superior electrochemical performances compared to TiN and conductive C_b electrodes (7.92% vs 6.59%) [127]. TiN/MC nanohybrid CEs in DSSCs resulted in a PCE of 8.41% with the I_3^-/I^- electrolyte system, greater than that of Pt CEs (8.0%). TiN/MC hybrid CE yielded a PCE of 6.71% in a T_2/T^- electrolyte DSSC system, higher than that of the Pt CE (3.32%). As compared to the Pt electrode, the chemical stability of TiN/MC hybrid CE in organic T_2/T^- electrolyte was also improved [128]. The unique structure feature and the synergistic effects between TMC and carbon materials should be responsible for superior photovoltaic performance in I- and T-mediated DSSCs.

The combination of TMCs into polymers can offer a synergistic catalytic effect on improving performance to I_3^- reduction in DSSCs. The CoS/PEDOT-PSS exhibited better catalytic activity by utilizing the merits of CoS and PEDOT-PSS films and yielded a PCE of 5.4%, comparable to that of the Pt electrode (6.1%) [129]. This work demonstrates improved catalytic properties that make CoS/PEDOT-PSS feasible for practical applications in lightweight and flexible devices. The typical synergistic effect is also illustrated in TiN/PEDOT-PSS hybrid CEs. Use of optimized composition and thickness of CE catalyst, the

TiN/PEDOT-PSS film as CE catalyst yielded a PCE of 6.67% in DSSCs with CYC-B1 dye, higher than that of DSSCs with a sputtered Pt electrode [130]. Further investigation demonstrated that the morphology plays a key role in improving photovoltaic performance of DSSCs. TiN nanoparticles (TiN(P)), TiN nanorods (TiN(R)), and TiN mesoporous spheres (TiN(S)) are incorporated into PEDOT-PSS. Use of TiN(P)/PEDOT-PSS as a CE in DSSCs produced a PCE of 7.06%, higher than that of TiN(R)/PEDOT-PSS (6.89%) and TiN(S)/PEDOT-PSS (6.19%) electrodes. In addition, these TiN/PEDOT-PSS as CEs in DSSCs presented much higher PCE values than those of DSSCs with PEDOT-PSS, TiN(P), TiN(R), and TiN(S) [131]. This design idea combines high electrical conductivity and superior catalytic activity of TiN and PEDOT-PSS, allowing that TiN/PEDOT-PSS provides more favorable and efficient interfacial active sites for I_3^- reduction.

The state-of-the-art design of three-component carbon/TMCs/polymer hybrids has exhibited the superior catalytic activity for I_3^- reduction. The Co/PPy/C (C: carbon) and Ni/PPy/C hybrids exhibit a higher catalytic activity to I_3^- reduction than Fe/PPy/C, which can attribute to the formation of the Co–N and Ni–N catalytic sites. The higher catalytic activity resulted in a PCE of 7.64%, higher than the Fe/PPy/C (5.07%), Ni/PPy/C (7.44%), and PPy/C (7.09%) electrodes [132]. In addition, the TiC/graphene/PEDOT-PSS hybrids used as CEs in flexible DSSCs yielded a PCE of 4.5%, slightly higher than that of a DSSC with Pt electrode (4.3%) [133]. The better adhesion of the TiC/graphene/PEDOT-PSS CE films to the flexible substrate resulted in better mechanical properties of the CE films, highly desirable for practical application.

Apart from the hybrid CEs mentioned above, the polycomponent, such as Cu_2ZnSnS_4 (CZTS), $Cu_2ZnSnSe_4$ (CZTSe), $NiCo_2S_4$, and CZTSe/MWCNTs, is another type of Pt-free hybrid CE materials [134–138]. The CZTS CE films after selenization presented an impressive catalytic activity to the I_3^- reduction, resulting in a PCE of 7.37% in DSSCs, close to that of the DSSCs with Pt electrode (7.04%). By contrast, the CZTSe as CE catalysts only exhibited a PCE of 3.85% in DSSCs. $CoMoS_4$- and $NiMoS_4$-based CEs yield PCE values >7% and showed similar photovoltaic performances to DSSCs with Pt CEs [138]. These polycomponent inorganic compounds are not very impressive as compared with two-component and three-component hybrids in DSSCs.

Another attractive hybrid is Pt-loaded hybrid CE materials. Carbon materials, conductive polymers, TMCs, and other metals were employed as support materials, as illustrated in Figure 1.4c. A small amount of Pt was loaded onto support materials to achieve similar catalytic properties to Pt electrode in DSSCs. The use of support materials in Pt-loaded hybrids is to prevent Pt nanoparticle aggregation and control the amount of Pt. Pt-loaded hybrid CE materials have been demonstrated to achieve the enhanced mechanical rigidity and chemical stability. Reported technical strategies to reduce dependence on Pt have been developed to produce Pt-free catalytic materials in the catalytic fields [55, 56, 60].

In general, all hybrid CE catalysts in DSSCs outperform their corresponding components, and the PCE of DSSCs can be greatly enhanced using hybrid CEs. The superior catalytic performance of hybrid CE catalysts can be attributed to the synergetic effects of the different components of the hybrid CE materials.

However, the exact reason for superior catalytic activity of the hybrids keeps unclear. On the other hand, the hybrid CE materials can be designed to meet the demands of new-system DSSCs with new components (dyes, electrolyte, and redox couples). However, matching and stability of CE catalyst and DSSC device are still the main limitations for their practical use. We believe that the hybrid CEs can pave the way for the development of high-performance and low-cost DSSCs in future.

1.6 General Design Consideration of this Book

High-speed development of third-generation solar cells resulted in an increasingly scientific papers published in the past two decades. As a critical component of DSSCs, the CE catalysts have become the focus of research that was mainly driven by desires to overcome the Pt challenges. In this context, we edit this book *Counter Electrodes for Dye-Sensitized and Perovskite Solar Cells* covering important contributions from different DSSC groups around the world by a selective presentation of recent research highlights. In this book, we focus on the design ideas, fabrication approaches, and characterization techniques of novel CE catalytic materials and stress the merits and demerits of well-designed carbon materials, conductive polymers, TMCs, and their corresponding hybrids. The prospects and challenges of alternative Pt catalysts for their practical applications in DSSCs were included.

Typical noble metal Pt catalyst was assigned in Chapter 2, and metal and alloy CE catalysts were assigned in Chapter 3 for I-mediated DSSCs. Subsequently, carbon materials including carbon/carbon nanohybrids, carbon nanotubes, and graphene CE catalyst were fixed in Chapters 4–6. TMCs including TMCs/TMC hybrids and conductive polymers including polymers/polymer hybrids were introduced in Chapters 7 and 8, respectively. After that, two-component, three-component, and polycomponent hybrid CE catalysts, such as Pt-loaded hybrid CEs, TMCs/carbon hybrids, TMCs/polymer hybrids, carbon/polymers hybrids, carbon/TMCs/polymers, were arranged in Chapters 9–13. As an alternative to the I_3^-/I^- redox couple, the T_2/T^- and Co^{2+}/Co^{3+} redox couples were given a special concern in T- and Co-mediated DSSCs in Chapters 14 and 15, respectively.

It is true that much more is now known about the principal physicochemical processes that occur during CE operation of the DSSCs, but the stability issues associated with CEs have not been matched by the exponential increase in CE research effort [57]. It should be noted that there is not enough data to evaluate the stability of a symmetrical dummy cell fabricated using two CE materials and the long-term stability of a DSSCs. This means that the stability might limit their possible commercial application. In this regard, the CE stability issue was specially addressed in Chapter 16, offering strategies to overcome the current stability stalemate.

As far as the TMCs are concerned, the catalytic activity is an intrinsic characteristic of a catalyst that is determined by the electronic structure of the catalyst. However, the accurate relationship between the electronic structure and

the catalytic activity remains unclear. No one knows for sure which electronic structure of CE materials can make them exhibit superior catalytic performance. For the hybrid CE catalysts, the superior catalytic activity can be attributed to the synergistic effect resulting from the different components of the hybrid CE materials. However, the clear role of each component in the hybrid materials remains unclear. This means that predicting which CE materials will exhibit superior catalytic activity in DSSCs is exceedingly difficult. The catalytic mechanism of TMCs as CE catalysts in DSSCs is not clear even though they exhibit superior catalytic activity. Therefore, the first-principle density functional theory (DFT) calculations and ab initio Car–Parrinello molecular dynamics (CPMD) simulations is highly desired for understanding the catalytical mechanism of TMCs in DSSCs.

Expect for DSSCs, several special issues on perovskite solar cells, for example, metal- and carbon-based contact electrodes, the first-principles DFT calculations, and boundary engineering contact for perovskite solar cells, were also included in Chapters 17–20 in this book. Finally, the *Cell Efficiency Table of DSSCs with Various Counter Electrode Electrocatalysts* was given in the Appendix. This book can be communicated to the wider scientific community to stimulate further progress of DSSCs and perovskite solar cells.

Acknowledgments

Financial support from NSFC (51672208), National Science & Technology Pillar Program during the Twelfth Five-year Plan Period (2012BAD47B02), Sci-Tech R&D Program of Shaanxi Province (2010K01-120 and 2015JM5183), and Shaanxi Provincial Department of Education (2013JK0927) is greatly acknowledged. The project was partly sponsored by SRF for ROCS, SEM.

References

1 Gerischer, H., Michel-Beyerle, M.E., Rebentrost, F., and Tributsch, H. (1968). Sensitization of charge injection into semiconductors with large band gap. *Electrochim. Acta* 13 (6): 1509–1515.
2 Gerischer, H. and Tributsch, H. (1968). Elektrochemische Untersuchungen zur spektralen Sensibilisierung von ZnO-Einkristallen. *Ber. Bunsenges. Phys. Chem.* 72 (3): 437–445.
3 Tributsch, H. and Gerischer, H. (1969). The use of semiconductor electrodes in the study of photochemical reactions. *Ber. Bunsen Ges. Phys. Chem.* 73 (8–9): 850–854.
4 Tributsch, H. (1972). Reaction of excited chlorophyll molecules at electrodes and in photosynthesis. *Photochem. Photobiol.* 16 (4): 261–269.
5 Tributsch, H. and Calvin, M. (1971). Electrochemistry of excited molecules: photo-electrochemical reactions of chlorophylls. *Photochem. Photobiol.* 14 (2): 95–112.
6 Clark, W.D.K. and Sutin, N. (1977). Spectral sensitization of n-type titanium dioxide electrodes by polypyridine ruthenium(II) complexes. *J. Am. Chem. Soc.* 99 (14): 4676–4682.

7 Gerischer, H. (1990). The impact of semiconductors on the concepts of electrochemistry. *Electrochim. Acta* 35 (11–12): 1677–1699.

8 Jaegermann, W. and Tributsch, H. (1988). Interfacial properties of semiconducting transition metal chalcogenides. *Prog. Surf. Sci.* 29 (1–2): 1–167.

9 Spitler, M.T. and Calvin, M. (1977). Electron transfer at sensitized TiO_2 electrodes. *J. Chem. Phys.* 66 (10): 4294–4305.

10 O'Regan, B. and Grätzel, M. (1991). A low-cost, high-efficiency solar cell based on dye-sensitized colloidal TiO_2 films. *Nature* 353 (6346): 737–740.

11 Ahmad, S., Guillen, E., Kavan, L. et al. (2013). Metal free sensitizer and catalyst for dye sensitized solar cells. *Energy Environ. Sci.* 6 (12): 3439–3466.

12 Brown, T.M., De Rossi, F., Di Giacomo, F. et al. (2014). Progress in flexible dye solar cell materials, processes and devices. *J. Mater. Chem. A* 2 (28): 10788–10817.

13 Grätzel, C. and Zakeeruddin, S.M. (2013). Recent trends in mesoscopic solar cells based on molecular and nanopigment light harvesters. *Mater. Today* 16 (1–2): 11–18.

14 Grätzel, M. (2001). Photoelectrochemical cells. *Nature* 414 (6861): 338–344.

15 Grätzel, M. (2004). Conversion of sunlight to electric power by nanocrystalline dye-sensitized solar cells. *J. Photochem. Photobiol., A* 164 (1–3): 3–14.

16 Grätzel, M. (2005). Dye-sensitized solid-state heterojunction solar cells. *MRS Bull.* 30 (1): 23–27.

17 Grätzel, M. (2005). Solar energy conversion by dye-sensitized photovoltaic cells. *Inorg. Chem.* 44 (20): 6841–6851.

18 Grätzel, M. (2009). Recent advances in sensitized mesoscopic solar cells. *Acc. Chem. Res.* 42 (11): 1788–1798.

19 Gratzel, M., Janssen, R.A., Mitzi, D.B., and Sargent, E.H. (2012). Materials interface engineering for solution-processed photovoltaics. *Nature* 488: 304–312.

20 Hagfeldt, A., Boschloo, G., Sun, L. et al. (2010). Dye-sensitized solar cells. *Chem. Rev.* 110 (11): 6595–6663.

21 Li, D., Qin, D., Deng, M. et al. (2009). Optimization the solid-state electrolytes for dye-sensitized solar cells. *Energy Environ. Sci.* 2 (3): 283–291.

22 Liang, M. and Chen, J. (2013). Arylamine organic dyes for dye-sensitized solar cells. *Chem. Soc. Rev.* 42 (8): 3453–3488.

23 Luo, Y., Li, D., and Meng, Q. (2009). Towards optimization of materials for dye-sensitized solar cells. *Adv. Mater.* 21 (45): 4647–4651.

24 Nogueira, A.F., Longo, C., and De Paoli, M.-A. (2004). Polymers in dye sensitized solar cells: overview and perspectives. *Coord. Chem. Rev.* 248 (13–14): 1455–1468.

25 Peter, L.M. (2011). The Grätzel cell: where next? *J. Phys. Chem. Lett.* 2 (15): 1861–1867.

26 Pettersson, H., Nonomura, K., Kloo, L., and Hagfeldt, A. (2012). Trends in patent applications for dye-sensitized solar cells. *Energy Environ. Sci.* 5 (6): 7376–7380.

27 Snaith, H.J. (2010). Estimating the maximum attainable efficiency in dye-sensitized solar cells. *Adv. Funct. Mater.* 20 (1): 13–19.

28 Snaith, H.J. and Schmidt-Mende, L. (2007). Advances in liquid-electrolyte and solid-state dye-sensitized solar cells. *Adv. Mater.* 19 (20): 3187–3200.

29 Sommeling, P.M., Späth, M., Smit, H.J.P. et al. (2004). Long-term stability testing of dye-sensitized solar cells. *J. Photochem. Photobiol., A* 164 (1–3): 137–144.

30 Tributsch, H. (2004). Dye sensitization solar cells: a critical assessment of the learning curve. *Coord. Chem. Rev.* 248 (13–14): 1511–1530.

31 Wu, J., Lan, Z., Lin, J. et al. (2015). Electrolytes in dye-sensitized solar cells. *Chem. Rev.* 115 (5): 2136–2173.

32 Yanagida, S., Yu, Y., and Manseki, K. (2009). Iodine/iodide-free dye-sensitized solar cells. *Acc. Chem. Res.* 42 (11): 1827–1838.

33 Ye, M., Wen, X., Wang, M. et al. (2015). Recent advances in dye-sensitized solar cells: from photoanodes, sensitizers and electrolytes to counter electrodes. *Mater. Today* 18 (3): 155–162.

34 Nazeeruddin, M.K., Kay, A., Rodicio, I. et al. (1993). Conversion of light to electricity by cis-X^2bis(2,2′-bipyridyl-4,4′-dicarboxylate)ruthenium(II) charge-transfer sensitizers (X = Cl-, Br-, I-, CN-, and SCN-) on nanocrystalline titanium dioxide electrodes. *J. Am. Chem. Soc.* 115 (14): 6382–6390.

35 Barbe, C.J., Arendse, F., Comte, P. et al. (1997). Nanocrystalline titanium oxide electrodes for photovoltaic applications. *J. Am. Ceram. Soc.* 80 (12): 3157–3171.

36 Nazeeruddin, M.K., De Angelis, F., Fantacci, S. et al. (2005). Combined experimental and DFT-TDDFT computational study of photoelectrochemical cell ruthenium sensitizers. *J. Am. Chem. Soc.* 127 (48): 16835–16847.

37 Chiba, Y., Islam, A., Watanabe, Y. et al. (2006). Dye-sensitized solar cells with conversion efficiency of 11.1%. *Jpn. J. Appl. Phys.* 45 (7L): L638–L640.

38 Chen, C.-Y., Wang, M., Li, J.-Y. et al. (2009). Highly efficient light-harvesting ruthenium sensitizer for thin-film dye-sensitized solar cells. *ACS Nano* 3 (10): 3103–3109.

39 Yu, Q., Wang, Y., Yi, Z. et al. (2010). High-efficiency dye-sensitized solar cells: the influence of lithium ions on exciton dissociation, charge recombination, and surface states. *ACS Nano* 4 (10): 6032–6038.

40 Han, L., Islam, A., Chen, H. et al. (2012). High-efficiency dye-sensitized solar cell with a novel co-adsorbent. *Energy Environ. Sci.* 5 (3): 6057–6060.

41 Horiuchi, T., Miura, H., Sumioka, K., and Uchida, S. (2004). High efficiency of dye-sensitized solar cells based on metal-free indoline dyes. *J. Am. Chem. Soc.* 126 (39): 12218–12219.

42 Ito, S., Zakeeruddin, S.M., Humphry-Baker, R. et al. (2006). High-efficiency organic-dye-sensitized solar cells controlled by nanocrystalline-TiO_2 electrode thickness. *Adv. Mater.* 18 (9): 1202–1205.

43 Ito, S., Miura, H., Uchida, S. et al. (2008). High-conversion-efficiency organic dye-sensitized solar cells with a novel indoline dye. *Chem. Commun.* (41): 5194–5196.

44 Zeng, W., Cao, Y., Bai, Y. et al. (2010). Efficient dye-sensitized solar cells with an organic photosensitizer featuring orderly conjugated ethylenedioxythiophene and dithienosilole blocks. *Chem. Mater.* 22 (5): 1915–1925.

45 Yella, A., Humphry-Baker, R., Curchod, B.F.E. et al. (2013). Molecular engineering of a fluorene donor for dye-sensitized solar cells. *Chem. Mater.* 25 (13): 2733–2739.

46 Kay, A. and Graetzel, M. (1993). Artificial photosynthesis. 1. Photosensitization of titania solar cells with chlorophyll derivatives and related natural porphyrins. *J. Phys. Chem.* 97 (23): 6272–6277.

47 Cherian, S. and Wamser, C.C. (2000). Adsorption and photoactivity of tetra(4-carboxyphenyl)porphyrin (TCPP) on nanoparticulate TiO_2. *J. Phys. Chem. B* 104 (15): 3624–3629.

48 Wang, Q., Campbell, W.M., Bonfantani, E.E. et al. (2005). Efficient light harvesting by using green Zn-porphyrin-sensitized nanocrystalline TiO_2 films. *J. Phys. Chem. B* 109 (32): 15397–15409.

49 Campbell, W.M., Jolley, K.W., Wagner, P. et al. (2007). Highly efficient porphyrin sensitizers for dye-sensitized solar cells. *J. Phys. Chem. C* 111 (32): 11760–11762.

50 Bessho, T., Zakeeruddin, S.M., Yeh, C.-Y. et al. (2010). Highly efficient mesoscopic dye-sensitized solar cells based on donor-acceptor-substituted porphyrins. *Angew. Chem. Int. Ed.* 49 (37): 6646–6649.

51 Yella, A., Lee, H.-W., Tsao, H.N. et al. (2011). Porphyrin-sensitized solar cells with cobalt (II/III)-based redox electrolyte exceed 12 percent efficiency. *Science* 334 (6056): 629–634.

52 Mathew, S., Yella, A., Gao, P. et al. (2014). Dye-sensitized solar cells with 13% efficiency achieved through the molecular engineering of porphyrin sensitizers. *Nat. Chem.* 6 (3): 242–247.

53 Kakiage, K., Aoyama, Y., Yano, T. et al. (2015). Highly-efficient dye-sensitized solar cells with collaborative sensitization by silyl-anchor and carboxy-anchor dyes. *Chem. Commun.* 51 (88): 15894–15897.

54 Hao, F., Dong, P., Luo, Q. et al. (2013). Recent advances in alternative cathode materials for iodine-free dye-sensitized solar cells. *Energy Environ. Sci.* 6 (7): 2003–2019.

55 Yun, S., Hagfeldt, A., and Ma, T. (2014). Pt-free counter electrode for dye-sensitized solar cells with high efficiency. *Adv. Mater.* 26 (36): 6210–6237.

56 Yun, S., Hagfeldt, A., and Ma, T. (2014). Superior catalytic activity of Sub-5 μm-thick Pt/SiC films as counter electrodes for dye-sensitized solar cells. *ChemCatChem* 6 (6): 1584–1588.

57 Yun, S., Lund, P.D., and Hinsch, A. (2015). Stability assessment of alternative platinum free counter electrodes for dye-sensitized solar cells. *Energy Environ. Sci.* 8 (12): 3495–3514.

58 Yun, S., Pu, H., Chen, J. et al. (2014). Enhanced performance of supported HfO_2 counter electrodes for redox couples used in dye-sensitized solar cells. *ChemSusChem* 7 (2): 442–450.

59 Yun, S., Wang, L., Guo, W., and Ma, T. (2012). Non-Pt counter electrode catalysts using tantalum oxide for low-cost dye-sensitized solar cells. *Electrochem. Commun.* 24 (0): 69–73.

60 Yun, S., Wang, L., Zhao, C. et al. (2013). A new type of low-cost counter electrode catalyst based on platinum nanoparticles loaded onto silicon

carbide (Pt/SiC) for dye-sensitized solar cells. *Phys. Chem. Chem. Phys.* 15 (12): 4286–4290.

61 Yun, S., Wu, M., Wang, Y. et al. (2013). Pt-like behavior of high-performance counter electrodes prepared from binary tantalum compounds showing high electrocatalytic activity for dye-sensitized solar cells. *ChemSusChem* 6 (3): 411–416.

62 Yun, S., Zhang, H., Pu, H. et al. (2013). Metal oxide/carbide/carbon nanocomposites: in situ synthesis, characterization, calculation, and their application as an efficient counter electrode catalyst for dye-sensitized solar cells. *Adv. Energy Mater.* 3 (11): 1407–1412.

63 Yun, S., Zhou, H., Wang, L. et al. (2013). Economical hafnium oxygen nitride binary/ternary nanocomposite counter electrode catalysts for high-efficiency dye-sensitized solar cells. *J. Mater. Chem. A* 1 (4): 1341–1348.

64 Zhang, T., Yun, S., Li, X. et al. (2017). Fabrication of niobium-based oxides/oxynitrides/nitrides and their applications in dye-sensitized solar cells and anaerobic digestion. *J. Power Sources* 340: 325–336.

65 Saygili, Y., Söderberg, M., Pellet, N. et al. (2016). Copper bipyridyl redox mediators for dye-sensitized solar cells with high photovoltage. *J. Am. Chem. Soc.* 138 (45): 15087–15096.

66 Papageorgiou, N. (2004). Counter-electrode function in nanocrystalline photoelectrochemical cell configurations. *Coord. Chem. Rev.* 248 (13–14): 1421–1446.

67 Tang, Y., Pan, X., Dai, S.Y. et al. (2011). Research progress of the counter electrode in dye-sensitized solar cells. *Key Eng. Mater.* 451: 63–78.

68 Thomas, S., Deepak, T.G., Anjusree, G.S. et al. (2014). A review on counter electrode materials in dye-sensitized solar cells. *J. Mater. Chem. A* 2 (13): 4474–4490.

69 Wu, M. and Ma, T. (2014). Recent progress of counter electrode catalysts in dye-sensitized solar cells. *J. Phys. Chem. C* 118 (30): 16727–16742.

70 Hwang, S., Batmunkh, M., Nine, M.J. et al. (2015). Dye-sensitized solar cell counter electrodes based on carbon nanotubes. *ChemPhysChem* 16 (1): 53–65.

71 Theerthagiri, J., Senthil, A.R., Madhavan, J., and Maiyalagan, T. (2015). Recent progress in non-platinum counter electrode materials for dye-sensitized solar cells. *ChemElectroChem* 2 (7): 928–945.

72 Wu, M. and Ma, T. (2012). Platinum-free catalysts as counter electrodes in dye-sensitized solar cells. *ChemSusChem* 5 (8): 1343–1357.

73 Yun, S., Freitas, J.N., Nogueira, A.F. et al. (2016). Dye-sensitized solar cells employing polymers. *Prog. Polym. Sci.* 59: 1–40.

74 Tang, Q., Duan, J., Duan, Y. et al. (2015). Recent advances in alloy counter electrodes for dye-sensitized solar cells. A critical review. *Electrochim. Acta* 178: 886–899.

75 Wei, W., Wang, H., and Hu, Y.H. (2014). A review on PEDOT-based counter electrodes for dye-sensitized solar cells. *Int. J. Energy Res.* 38 (9): 1099–1111.

76 Wu, M., Lin, X., Wang, Y., and Ma, T. (2015). Counter electrode materials combined with redox couples in dye- and quantum dot-sensitized solar cells. *J. Mater. Chem. A* 3 (39): 19638–19656.

77 Yun, S., Liu, Y., Zhang, T., and Ahmad, S. (2015). Recent advances in alternative counter electrode materials for co-mediated dye-sensitized solar cells. *Nanoscale* 7 (28): 11877–11893.

78 Zhang, T., Liu, Y., and Yun, S. (2015). Recent advances in counter electrodes for thiolate-mediated dye-sensitized solar cells. *Israel J. Chem.* 55 (9): 943–954.

79 Esposito, D.V., Hunt, S.T., Kimmel, Y.C., and Chen, J.G. (2012). A new class of electrocatalysts for hydrogen production from water electrolysis: metal monolayers supported on low-cost transition metal carbides. *J. Am. Chem. Soc.* 134 (6): 3025–3033.

80 Hwu, H.H. and Chen, J.G. (2004). Surface chemistry of transition metal carbides. *Chem. Rev.* 105 (1): 185–212.

81 Roy-Mayhew, J.D. and Aksay, I.A. (2014). Graphene materials and their use in dye-sensitized solar cells. *Chem. Rev.* 114 (12): 6323–6348.

82 Nam, J.G., Park, Y.J., Kim, B.S., and Lee, J.S. (2010). Enhancement of the efficiency of dye-sensitized solar cell by utilizing carbon nanotube counter electrode. *Scr. Mater.* 62 (3): 148–150.

83 Furimsky, E. (2003). Metal carbides and nitrides as potential catalysts for hydroprocessing. *Appl. Catal., A* 240 (1–2): 1–28.

84 Levy, R.B. and Boudart, M. (1973). Platinum-like behavior of tungsten carbide in surface catalysis. *Science* 181 (4099): 547–549.

85 Liu, Y., Yun, S., Zhou, X. et al. (2017). Intrinsic origin of superior catalytic properties of tungsten-based catalysts in dye-sensitized solar cells. *Electrochim. Acta* 242 (Suppl. C): 390–399.

86 Zhou, H., Shi, Y., Wang, L. et al. (2013). Notable catalytic activity of oxygen-vacancy-rich $WO_{2.72}$ nanorod bundles as counter electrodes for dye-sensitized solar cells. *Chem. Commun.* 49 (69): 7626–7628.

87 Lin, X., Wu, M.X., Wang, Y. et al. (2011). Novel counter electrode catalysts of niobium oxides supersede Pt for dye-sensitized solar cells. *Chem. Commun.* 47 (41): 11489–11491.

88 Wu, M., Lin, X., Hagfeldt, A., and Ma, T. (2011). Low-cost molybdenum carbide and tungsten carbide counter electrodes for dye-sensitized solar cells. *Angew. Chem. Int. Ed.* 50 (15): 3520–3524.

89 Wu, M., Lin, X., Wang, Y. et al. (2012). Economical Pt-free catalysts for counter electrodes of dye-sensitized solar cells. *J. Am. Chem. Soc.* 134 (7): 3419–3428.

90 Li, G.R., Song, J., Pan, G.L., and Gao, X.P. (2011). Highly Pt-like electrocatalytic activity of transition metal nitrides for dye-sensitized solar cells. *Energy Environ. Sci.* 4 (5): 1680–1683.

91 Jiang, Q.W., Li, G.R., and Gao, X.P. (2009). Highly ordered TiN nanotube arrays as counter electrodes for dye-sensitized solar cells. *Chem. Commun.* (44): 6720–6722.

92 Zhang, X., Chen, X., Dong, S. et al. (2012). Hierarchical micro/nano-structured titanium nitride spheres as a high-performance counter electrode for a dye-sensitized solar cell. *J. Mater. Chem.* 22 (13): 6067–6071.

93 Burschka, J., Brault, V., Ahmad, S. et al. (2012). Influence of the counter electrode on the photovoltaic performance of dye-sensitized solar cells using a disulfide/thiolate redox electrolyte. *Energy Environ. Sci.* 5 (3): 6089–6097.

94 Chang, S.-H., Lu, M.-D., Tung, Y.-L., and Tuan, H.-Y. (2013). Gram-scale synthesis of catalytic Co_9S_8 nanocrystal ink as a cathode material for spray-deposited, large-area dye-sensitized solar cells. *ACS Nano* 7 (10): 9443–9451.

95 Huang, Q.-H., Ling, T., Qiao, S.-Z., and Du, X.-W. (2013). Pyrite nanorod arrays as an efficient counter electrode for dye-sensitized solar cells. *J. Mater. Chem. A* 1 (38): 11828–11833.

96 Kung, C.-W., Chen, H.-W., Lin, C.-Y. et al. (2012). CoS acicular nanorod arrays for the counter electrode of an efficient dye-sensitized solar cell. *ACS Nano* 6 (8): 7016–7025.

97 Mulmudi, H.K., Batabyal, S.K., Rao, M. et al. (2011). Solution processed transition metal sulfides: application as counter electrodes in dye sensitized solar cells (DSCs). *Phys. Chem. Chem. Phys.* 13 (43): 19307–19309.

98 Wang, M., Anghel, A.M., Marsan, B. et al. (2009). CoS supersedes Pt as efficient electrocatalyst for triiodide reduction in dye-sensitized solar cells. *J. Am. Chem. Soc.* 131 (44): 15976–15977.

99 Wang, Y.-C., Wang, D.-Y., Jiang, Y.-T. et al. (2013). FeS_2 nanocrystal Ink as a catalytic electrode for dye-sensitized solar cells. *Angew. Chem. Int. Ed.* 52 (26): 6694–6698.

100 Wu, M., Wang, Y. et al. (2011). Economical and effective sulfide catalysts for dye-sensitized solar cells as counter electrodes. *Phys. Chem. Chem. Phys.* 13 (43): 19298–19301.

101 Gong, F., Wang, H., Xu, X. et al. (2012). In situ growth of $Co_{0.85}Se$ and $Ni_{0.85}Se$ on conductive substrates as high-performance counter electrodes for dye-sensitized solar cells. *J. Am. Chem. Soc.* 134 (26): 10953–10958.

102 Gong, F., Xu, X., Li, Z. et al. (2013). $NiSe_2$ as an efficient electrocatalyst for a Pt-free counter electrode of dye-sensitized solar cells. *Chem. Commun.* 49 (14): 1437–1439.

103 Dou, Y.Y., Li, G.R., Song, J., and Gao, X.P. (2012). Nickel phosphide-embedded graphene as counter electrode for dye-sensitized solar cells. *Phys. Chem. Chem. Phys.* 14 (4): 1339–1342.

104 Wu, M., Bai, J., Wang, Y. et al. (2012). High-performance phosphide/carbon counter electrode for both iodide and organic redox couples in dye-sensitized solar cells. *J. Mater. Chem.* 22 (22): 11121–11127.

105 Qin, Q., Tao, J., Yang, Y., and Dong, X. (2011). In situ oxidative polymerization of polyaniline counter electrode on ITO conductive glass substrate. *Polym. Eng. Sci.* 51 (4): 663–669.

106 Saito, Y., Kubo, W., Kitamura, T. et al. (2004). I^-/I_3^- redox reaction behavior on poly(3,4-ethylenedioxythiophene) counter electrode in dye-sensitized solar cells. *J. Photochem. Photobiol., A* 164 (1–3): 153–157.

107 Li, Q., Wu, J., Tang, Q. et al. (2008). Application of microporous polyaniline counter electrode for dye-sensitized solar cells. *Electrochem. Commun.* 10 (9): 1299–1302.

108 Wang, H., Feng, Q., Gong, F. et al. (2013). In situ growth of oriented polyaniline nanowires array for efficient cathode of Co(iii)/Co(ii) mediated dye-sensitized solar cell. *J. Mater. Chem. A* 1 (1): 97–104.

109 Ahmad, S., Yum, J.-H., Butt, H.-J. et al. (2010). Efficient platinum-free counter electrodes for dye-sensitized solar cell applications. *ChemPhysChem* 11 (13): 2814–2819.

110 Yum, J.-H., Baranoff, E., Kessler, F. et al. (2012). A cobalt complex redox shuttle for dye-sensitized solar cells with high open-circuit potentials. *Nat. Commun.* 3: 631.

111 Pringle, J.M., Armel, V., and MacFarlane, D.R. (2010). Electrodeposited PEDOT-on-plastic cathodes for dye-sensitized solar cells. *Chem. Commun.* 46 (29): 5367–5369.

112 Trevisan, R., Döbbelin, M., Boix, P.P. et al. (2011). PEDOT nanotube arrays as high performing counter electrodes for dye sensitized solar cells. Study of the interactions among electrolytes and counter electrodes. *Adv. Energy Mater.* 1 (5): 781–784.

113 Lee, T.H., Do, K., Lee, Y.W. et al. (2012). High-performance dye-sensitized solar cells based on PEDOT nanofibers as an efficient catalytic counter electrode. *J. Mater. Chem.* 22 (40): 21624–21629.

114 Biallozor, S. and Kupniewska, A. (2000). Study on poly(3,4-ethylenedioxythiophene) behaviour in the I^-/I_2 solution. *Electrochem. Commun.* 2 (7): 480–486.

115 Tsao, H.N., Burschka, J., Yi, C. et al. (2011). Influence of the interfacial charge-transfer resistance at the counter electrode in dye-sensitized solar cells employing cobalt redox shuttles. *Energy Environ. Sci.* 4 (12): 4921–4924.

116 Lee, K.-M., Chen, P.-Y., Hsu, C.-Y. et al. (2009). A high-performance counter electrode based on poly(3,4-alkylenedioxythiophene) for dye-sensitized solar cells. *J. Power Sources* 188 (1): 313–318.

117 Li, Z., Ye, B., Hu, X. et al. (2009). Facile electropolymerized-PANI as counter electrode for low cost dye-sensitized solar cell. *Electrochem. Commun.* 11 (9): 1768–1771.

118 Xia, J., Masaki, N., Jiang, K., and Yanagida, S. (2007). The influence of doping ions on poly(3,4-ethylenedioxythiophene) as a counter electrode of a dye-sensitized solar cell. *J. Mater. Chem.* 17 (27): 2845–2850.

119 Lee, K.-M., Hsu, C.-Y., Chen, P.-Y. et al. (2009). Highly porous PProDOT-Et_2 film as counter electrode for plastic dye-sensitized solar cells. *Phys. Chem. Chem. Phys.* 11 (18): 3375–3379.

120 Tai, Q., Chen, B., Guo, F. et al. (2011). In situ prepared transparent polyaniline electrode and its application in bifacial dye-sensitized solar cells. *ACS Nano* 5 (5): 3795–3799.

121 Li, Y., Feng, Q., Wang, H. et al. (2013). Reduced graphene oxide–Ta_3N_5 composite: a potential cathode for efficient $Co(bpy)_3^{3+/2+}$ mediated dye-sensitized solar cells. *J. Mater. Chem. A* 1 (21): 6342–6349.

122 Li, Y., Wang, H., Feng, Q. et al. (2013). Reduced graphene oxide–TaON composite as a high-performance counter electrode for $Co(bpy)_3^{3+/2+}$-mediated dye-sensitized solar cells. *ACS Appl. Mater. Interfaces* 5 (16): 8217–8224.

123 Li, Z., Gong, F., Zhou, G., and Wang, Z.-S. (2013). NiS_2/reduced graphene oxide nanocomposites for efficient dye-sensitized solar cells. *J. Phys. Chem. C* 117 (13): 6561–6566.

124 Wu, M., Lin, X., Hagfeldt, A., and Ma, T. (2011). A novel catalyst of WO_2 nanorod for the counter electrode of dye-sensitized solar cells. *Chem. Commun.* 47 (15): 4535–4537.

125 Wu, M., Lin, X., Wang, L. et al. (2011). In situ synthesized economical tungsten dioxide imbedded in mesoporous carbon for dye-sensitized solar cells as counter electrode catalyst. *J. Phys. Chem. C* 115 (45): 22598–22602.

126 Li, G.R., Wang, F., Jiang, Q.-W. et al. (2010). Carbon nanotubes with titanium nitride as a low-cost counter-electrode material for dye-sensitized solar cells. *Angew. Chem. Int. Ed.* 49 (21): 3653–3656.

127 Li, G.R., Wang, F., Song, J. et al. (2012). TiN-conductive carbon black composite as counter electrode for dye-sensitized solar cells. *Electrochim. Acta* 65 (0): 216–220.

128 Ramasamy, E., Jo, C., Anthonysamy, A. et al. (2012). Soft-template simple synthesis of ordered mesoporous titanium nitride-carbon nanocomposite for high performance dye-sensitized solar cell counter electrodes. *Chem. Mater.* 24 (9): 1575–1582.

129 Sudhagar, P., Nagarajan, S., Lee, Y.-G. et al. (2011). Synergistic catalytic effect of a composite (CoS/PEDOT:PSS) counter electrode on triiodide reduction in dye-sensitized solar cells. *ACS Appl. Mater. Interfaces* 3 (6): 1838–1843.

130 Yeh, M.-H., Lin, L.-Y., Lee, C.-P. et al. (2011). A composite catalytic film of PEDOT:PSS/TiN–NPs on a flexible counter-electrode substrate for a dye-sensitized solar cell. *J. Mater. Chem.* 21 (47): 19021–19029.

131 Xu, H., Zhang, X., Zhang, C. et al. (2012). Nanostructured titanium nitride/PEDOT:PSS composite films as counter electrodes of dye-sensitized solar cells. *ACS Appl. Mater. Interfaces* 4 (2): 1087–1092.

132 Liu, G., Li, X., Wang, H. et al. (2013). A class of carbon supported transition metal–nitrogen complex catalysts for dye-sensitized solar cells. *J. Mater. Chem. A* 1 (4): 1475–1480.

133 Peng, Y., Zhong, J., Wang, K. et al. (2013). A printable graphene enhanced composite counter electrode for flexible dye-sensitized solar cells. *Nano Energy* 2 (2): 235–240.

134 Du, Y.F., Fan, J.Q., Zhou, W.-H. et al. (2012). One-step synthesis of stoichiometric $Cu_2ZnSnSe_4$ as counter electrode for dye-sensitized solar cells. *ACS Appl. Mater. Interfaces* 4 (3): 1796–1802.

135 Lin, J.-Y. and Chou, S.-W. (2013). Highly transparent $NiCo_2S_4$ thin film as an effective catalyst toward triiodide reduction in dye-sensitized solar cells. *Electrochem. Commun.* 37 (0): 11–14.

136 Xin, X., He, M., Han, W. et al. (2011). Low-cost copper zinc tin sulfide counter electrodes for high-efficiency dye-sensitized solar cells. *Angew. Chem. Int. Ed.* 50 (49): 11739–11742.

137 Zeng, X., Xiong, D., Zhang, W. et al. (2013). Spray deposition of water-soluble multiwall carbon nanotube and $Cu_2ZnSnSe_4$ nanoparticle composites as highly efficient counter electrodes in a quantum dot-sensitized solar cell system. *Nanoscale* 5 (15): 6992–6998.

138 Zheng, X., Guo, J., Shi, Y. et al. (2013). Low-cost and high-performance $CoMoS_4$ and $NiMoS_4$ counter electrodes for dye-sensitized solar cells. *Chem. Commun.* 49 (83): 9645–9647.